Heat Capacity Measurement by Flow Calorimetry: An Exact Analysis

T. K. Hei and J. D. Raal
School of Chemical Engineering, University of Kwa-Zulu Natal, King George V Avenue, Durban 4041, South Africa

DOI 10.1002/aic.11685
Published online November 25, 2008 in Wiley InterScience (www.interscience.wiley.com).

The principal unsolved problem in flow calorimetry for liquid heat capacity measurement accurate accounting for heat loss from the heater lead-in wires as a function of system properties is analyzed by exact procedures for a five-zone calorimeter model. Temperature distributions in the fluid, and bi-metal wire are obtained from solutions of the governing third-order ODE in the fluid temperature for realistic boundary conditions. Conductive heat losses at the fluid exit $q_{HL}/\dot{q}$ are large (up to 20% of energy input), and physical property and flow rate dependent. A new correlating equation for $(q_{HL}/\dot{q})$ gives separately and explicitly, for the first time, its dependence on calorimeter characteristics, flow rates and fluid properties. Experiments on five pure liquids confirmed the predictions of the theoretical model and produced Cp values in close agreement with literature data. Fluid friction and small convection heat losses $(U_iA_i\ (\Delta T)_{lm})$ were accounted for experimentally. © 2008 American Institute of Chemical Engineers *AIChE J,* 55: 206–216, 2009

Keywords: heat capacity measurement, flow, exact analysis

Introduction

Design procedures for heat-transfer equipment generally require values for the Prandtl number $Pr(=Cp\mu/k)$ as a function of temperature for pure liquids and liquid mixtures. Calculation of the evaporation ratio by new techniques (for exact determination of limiting activity coefficients by differential ebulliometry), requires precise values of solvent *Cp*, and latent heat as functions of temperature (Raal et al.[1]). Large collections of liquid heat capacity data (e.g., Zabransky et al.[2] and Domalski and Hearing[3]) are available in the literature, but for many liquids reliable data will not be available or may be uncertain due to discrepancies in reported values. For mixtures no reliable prediction procedures in terms of pure component values appear to be available. Prediction procedures for pure liquids are proposed and evaluated by Poling et al.[4] based on group contribution methods or corresponding states procedures. These procedures can give considerable errors for certain groups of compounds or at high-reduced temperatures. A sophisticated C_P^L prediction procedure has recently been developed by Diedrichs and Gmehling[5] based on a modified group contribution (VTPR) Peng -Robinson EOS. C_p is related, from its definition as an enthalpy derivative, to PVT properties and their derivatives through easily derived exact equations. Very good predictions were obtained for a substantial number of components.

Heat capacities are now frequently measured with commercial instruments (e.g., TA. Instruments, Tian- Calvet calorimeter (Settaram)), based on differential scanning (DSC) techniques. Recent heat-capacity measurements on ionic liquids by Diedrichs and Gmehling[6] using DSC and the more rapid "modulated-temperature DSC" methods, showed differences of up to 5% for the two techniques. Fairly extensive calibration procedures are required. Flow calorimeters have a comparatively rapid response, and the absence of any vapor space excludes thermal effects from evaporative processes.

In a simple flow calorimeter the temperature rise in a flowing liquid is measured for a given electrical power input from a heater element immersed in the fluid (or in contact with the walls of the flow-tube). Although a high-degree of

Correspondence concerning this article should be addressed to J. D. Raal at raal@ukzn.ac.za.

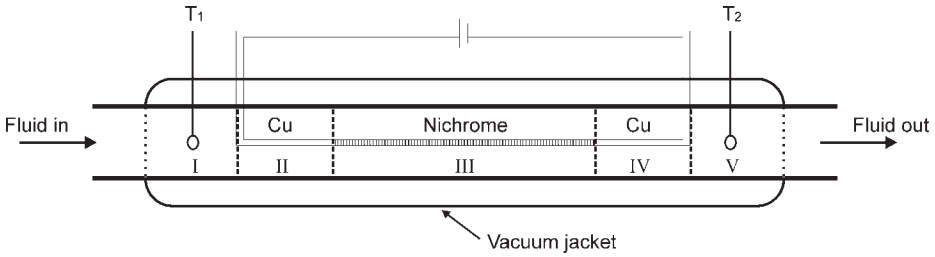

Figure 1. Schematic diagram of flow calorimeter.

insulation of the flow tube is possible (e.g., by vacuum jacketing), some heat loss through the heater lead-in wires is unavoidable. (see Figure 1). Since the lead-in wires (typically platinum or copper) must have high-electrical conductivity to ensure that there is energy generation only in the central nichrome element, they also provide a ready conductive path for heat loss to the surroundings. Quantification of this and other heat losses as a function of fluid flow rate and physical properties has been the subject of considerable effort by many investigators, and remains the principal problem in flow calorimentry for heat capacity measurement. (In flow calorimetry for excess enthalpy measurement, the principal problem becomes elimination or subtraction of frictional heating, again a function of fluid physical properties, from the measured mixing effect (Raal and Webley,[7] Raal[8]).

Many flow calorimeters currently in use are developments or variations of the differential calorimeters pioneered by Picker et al.[9] and Picker.[10] The former instrument is a differential one in which the power inputs required to maintain the final temperature equal in the working and reference arms are compared. To ensure consistency of flow rate the sample liquid is displaced by a reference liquid flowing through the same path. A disadvantage of this procedure is that some mixing of the sample and reference liquids is unavoidable and introduces, among others, errors due to heat of mixing effects. A major assumption, however, is that heat losses, for example from the electrical heater leads, are independent of fluid properties.

In earlier work Smith-McGowan and Wood[11] using a similar principle, incorporated a heat loss factor f in their calculations, and found f to be a function of calorimeter temperature. Other attempts at calculating or eliminating the effect of heat losses were made by Rogers and Pitzer,[12] Rogers and Duffy,[13] Saitoh et al.[14] and Nakagawa et al.[15] The latter researchers found heat losses to be only a mild function of flow rate for the liquids studied. The aforementioned procedures and several other often ingenious similar ones for flow or batch calorimeters account for heat losses by essentially *ad hoc* procedures, and do not provide insight into the dependence on fluid flow rate and physical properties. Also, the influence of fluid friction is not analyzed. It is the purpose of this publication to examine heat loss in a model flow calorimeter as a heat-transfer problem by exact analysis. Results are presented from studies on a variety of fluids, measured over widely varying flow rates and power inputs.

Mathematical Formulation

In Figure 1 a five-zone flow calorimeter is shown. Heat is generated electrically only in zone 3, and is transferred to the flowing fluid by convection characterized by the heat-transfer coefficient h. In zones 2 and 4 there is axial heat conduction along the lead-in wires of low-electrical resistance, but high-thermal conductivity (e.g., copper or platinum). Zones 1 and 5 correspond to a region, where the wire temperature has reached the environment temperature T_c and $h = o$.

Assuming only 1-D (one-dimensional) axial conduction in the heater, and the lead-in wire elements, an energy balance on a differential element dx of the solid conductor gives

$$\frac{d^2t}{dx^2} + \frac{\dot{q}Pf^2}{ka} - \frac{hPf^2}{ka}(t - T) = 0 \tag{1}$$

where T is the fluid temperature, P is the wire perimeter, t is the wire temperature, q is the power input per unit surface area of wire (W/m^2), k is the wire thermal conductivity (W/mK), and a is the wire cross-sectional area.

To permit extension to the practical case were the heater wire is coiled, the constant factor $f = dl/dx$ is introduced (1 = actual length of the wire). For zones 1, 2, 4 and 5 there is no heat generation and the second term is eliminated in Eq. 1.

Application of the first law of thermodynamics to steady-state flow in the annular area of a horizontal tube, for a differential element dx gives, (for 1-D flow)

$$(t - T) = \frac{C_H}{hPf}\frac{dT}{dx} + \frac{U}{hPf}\frac{dA}{dx}(T - T_C) \tag{2}$$

where C_H is the fluid thermal capacity $\dot{m}C_P$, A is the interior tube-wall area, U is the overall heat-transfer coefficient for heat loss (if any) through the tube wall to the surroundings, T is the fluid temperature, h is the heat-transfer coefficient for heat transfer from the wire surface to the fluid.

Note that Eq. 2 makes allowance (through U) for heat losses other than through the heater lead-in wires. It has been assumed that the fluid enthalpy is independent of pressure.

Equations 1 and 2 are coupled and can be reduced to a single third-order O.D.E. with constant coefficients by double differentiation of Eq. 2, with respect to x, and substitution into Eq. 1

$$\frac{d^3T}{dx^3} + \left(\frac{hPf}{C_H} + \frac{U}{C_H}\frac{dA}{dx}\right)\frac{d^2T}{dx^2} - \frac{hPf^2}{ka}\frac{dT}{dx} + \frac{\dot{q}hP^2f^3}{kaC_H} - \frac{UhPf^2}{kaC_H}\frac{dA}{dx}(T - T_C) = 0 \tag{3}$$

Equation 3 with only minor assumptions governs heat losses in a flow calorimeter of the kind shown in Figure 1.

Since the calorimeter is insulated with a vacuum jacket, the terms containing U are neglected since their inclusion makes the solution of Eq. 3 nearly intractable. Solution of Eq. 3 for $U \neq$ o can be obtained in principle by iterative procedures, for example by expressing $U_i A_i (T - T_C)$ as a polynomial in distance x, but such additional complexity does not seem worthwhile.

Solution of Equations

To broaden the solutions to apply to dimensionally similar calorimeters of any size, the equations(s) and the boundary conditions are rendered dimensionless by normalizing the temperature and distance with respect to $(T - T_C)_{ideal}$ and Δx_3 (= heated length as shown in Figure 1.) $(T - T_C)_{ideal}$ represents a situation of no heat losses, so

$$\overline{T} = \frac{T - T_C}{(T - T_C)_{ideal}} \tag{4}$$

(This follows a suggestion by C. J. Brouckaert,[16] and should render the equation and solutions independent of the environment temperature T_C)

$(T - T_C)_{ideal} (= \dot{q}/\dot{m}Cp)$ represents a situation of no heat losses.

Also

$$\bar{t} = \frac{t - T_c}{(T - T_c)_{ideal}} \tag{5}$$

and

$$\overline{x} = \frac{x}{\Delta x_3} (\Delta x_3 = x_3 - x_2 = \text{heated length}) \tag{6}$$

The dimensionless form of Eq. 3 (together with corresponding nondimensional boundary conditions) is given in Appendix 1. The boundary conditions enforced at the zone boundaries required that there be no discontinuities in temperature or heat flux in passing form one zone to another.

Solutions of Eq. 3 (Appendix 1)

For the case of $U = 0$, the governing third-order differential equation in the fluid temperature $\overline{T}$, can be reduced to an ordinary differential equation with constant coefficients since it does not contain the dependent variable $\overline{T}$, explicitly. The solution then becomes straightforward. For the central heated region (zone 3) for example one obtains

$$\overline{T} = C_4 \frac{e^{-q_1' \vec{x}}}{-q_1'} + C_5 \frac{e^{q_2' \bar{x}}}{q_2'} + \dot{q} \frac{\Delta x_3 Pf}{C_H T_{ref}} \overline{x} + C_6 \tag{7}$$

where the q_i are dimensionless quantities containing physical properties and calorimeter characteristics, all contained in the three dimensionless groups (see Appendix 1)

$$B = \left(\frac{hPf \Delta x_3}{C_H} \right)$$

$$m_1^2 = \left(\frac{hPf^2 (\Delta x_3)^2}{k_1 a} \right) \qquad [k_1 : copper]$$

$$m_2^2 = \left(\frac{hPf^2 (\Delta x_3)^2}{k_2 a} \right) \qquad [k_2 : nichrome]$$

For zones other than 3, $\dot{q} = 0$, and the thermal conductivity of the lead -in wires replaces that of the heater metal. Similar, but simpler solutions are obtained for these zones and involve several additional integration constants. The application of the boundary conditions, thus, produces a large system of linear equations containing 13 integration constants C_1 to C_{13}. The matrix of equations is shown in Appendix 2.

Temperature Profiles

Evaluation of the integration constants in the matrix for a particular fluid and a calorimeter with given dimensions (i.e., specified values of the dimensionless groups B and m_2 (or m_1) yields both dimensionless temperature profiles and lead-in wire conduction losses, the latter from

$$q_{x=x_1} = -k_1 a \left(\frac{dt}{dx} \right)_{x=x_1} \tag{8a}$$

$$q_{x=x_5} = -k_1 a \left(\frac{dt}{dx} \right)_{x=x_5} \tag{8b}$$

Typical fluid and wire temperature profiles are shown in Figure 2 for a fluid with the properties of n-hexane. It is evident that the conductive heat loss at the exit (Eq. 8b) is large, and that it completely overshadows that at the fluid entrance. This is a general conclusion.

Conduction heat losses

From Eq. 8b, the conductive heat loss at the exit is readily shown to be

$$q_{x=x_5} = \frac{-k_1 a \dot{q}}{(\Delta x_3)(\dot{m} C_P)} \cdot C_{11} \tag{9}$$

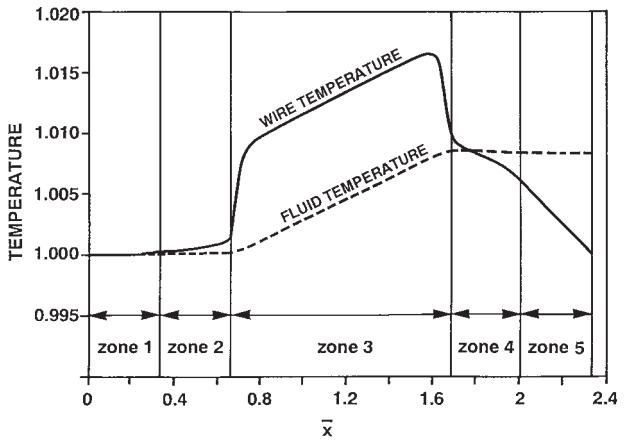

Figure 2. Nondimensional fluid and wire temperatures vs. $\overline{x}$ for a fluid with the properties of n-hexane.

Computed from Eq. 7, with constants obtained from inversion of the matrix (Appendix 2).

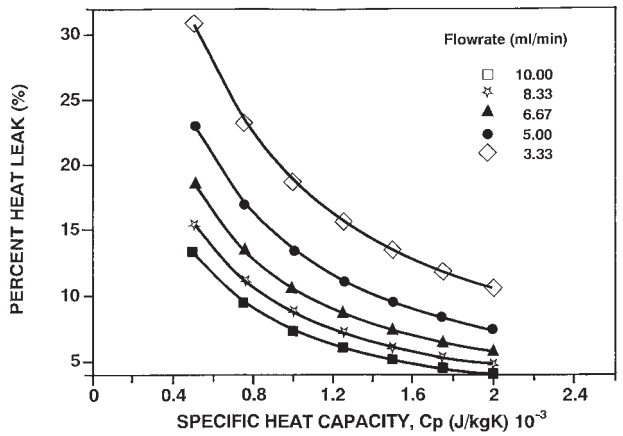

Figure 3. Conductive heat loss ($q_{HL}/\dot{q}$) as a function of fluid heat capacity *Cp*, for several flow rates, computed from Eq. 10.

Properties (other than *Cp*) are those of n-hexane. Calorimeter characteristics, $X = 3.5$.

Equation 9, however, provides no direct guidance on the conductive heat loss as a function of flow rate, physical properties and calorimeters characteristics, the main goal of the study. From the equations and boundary conditions for zones 3 and 4, it can, however, be shown (after extensive algebra) that the dimensionless conductive heat loss is given by

$$\frac{q_{HL}}{\dot{q}} = \frac{1}{X\sqrt{h}}\left\{C_8 e^{-X\sqrt{h}.\bar{x}_4} - C_9 e^{X\sqrt{h}.\bar{x}_4}\right\} \tag{10}$$

where

$$\mathrm{X} = \sqrt{\frac{\mathrm{P}(\Delta x_3)^2}{k_1 a}} \tag{11}$$

The two integration constants C_8 and C_9, which are fluid property and flow rate dependent, can in principle be obtained by solving the matrix in Appendix 2, but constructing the matrix without error requires considerable effort and care. The computer solutions, however, cannot give an explicit dependence of C_8 and C_9 on $\dot{V}$ and physical properties. A more attractive and user-friendly alternative was, therefore, found as follows.

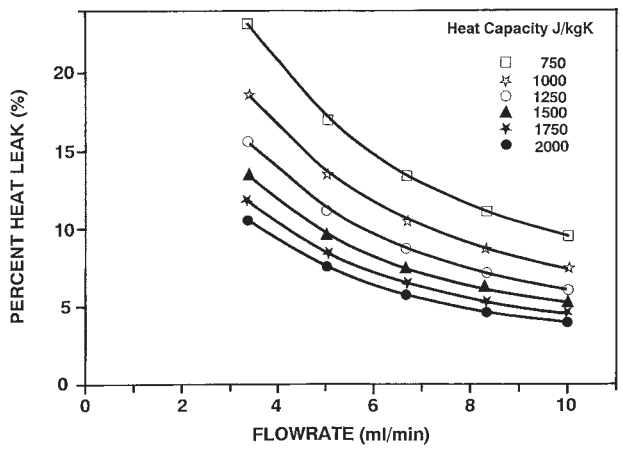

Figure 4. Conductive heat loss $q_{HL}/\dot{q}$ as a function flow rate for various assumed heat capacities, computed from Eq. 10.

Calorimeter characteristics, $X = 3.5$.

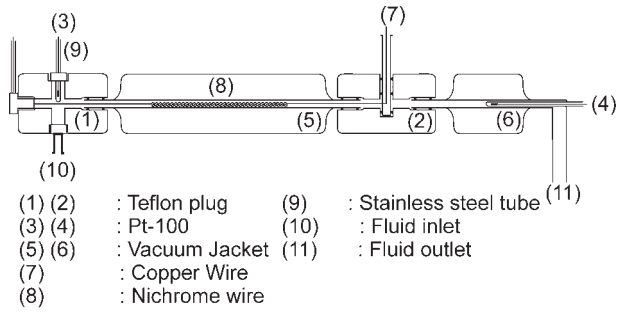

Figure 5. Schematic diagram of flow calorimeter, original design.

From the computer solutions for a range of flow rates satisfactory correlations were found as

$$C_8 = C_8'(\dot{V})^{n_8} \text{ and } C_9 = C_9'\left\{\frac{h}{\dot{V}\rho C_{\mathrm{P}}}\right\}^{n_9}$$

Using experimental measurements of q_{LH} for n-propanol and n-hexane (by the methods described following) for a range of flow rates, the two exponents were found to be $n_8 = 2.2$ and $n_9 = 2.47$. Eq. 10, thus, becomes finally

$$\frac{q_{HL}}{\dot{q}} = \frac{1}{X\sqrt{h}}\left\{C_8'(\dot{V})^{2.2} e^{-X\sqrt{h}.\bar{x}_4} - C_9'\left(\frac{h}{\dot{V}\rho C_{\mathrm{P}}}\right)^{2.47} e^{X\sqrt{h}.\bar{x}_4}\right\} \tag{12}$$

Although Eq. 12 now incorporates an empirical correlation for the two integration constants C_8 and C_9, it has produced a very useful form in which all fluid properties are incorporated in the convective heat-transfer coefficient h, and in the two constants C_8 and C_9, and the calorimeter characteristics in the group X.

Once determined from experiments with a fluid of known physical properties, the characterizing parameter X should

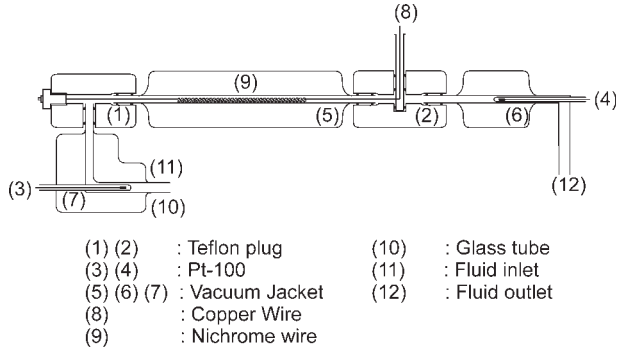

Figure 6. Schematic diagram of improved flow calorimeter.

Note modification of entrance section for improved inlet temperature measurement.

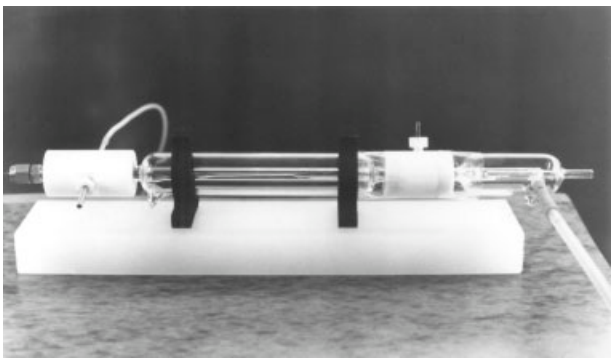

Figure 7. Photograph of glass and Teflon flow calorimeter.

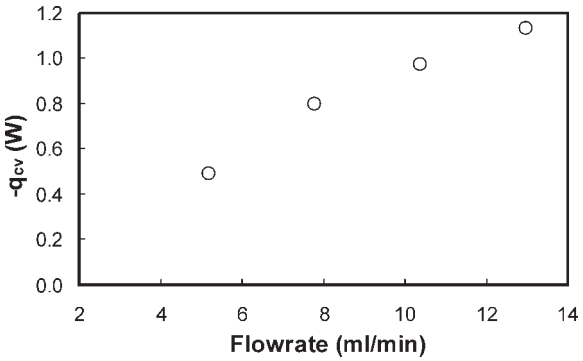

Figure 9. Measured convective heat loss ($q_{cv} = U_iA_i(\Delta T)_{LM}$) as a function of flow rate for n-heptane.

then remain constant for measurements with any other liquid, and independent of operating variables ($\dot{V}, \dot{q}$).

Correlating Equation for the Heat-Transfer Coefficient h

A suitable correlation for convective heat transfer for laminar flow in an annulus, with allowance for developing flow in the entrance region, is that of Mills[17]

$$Nu_m = 3.66 + \frac{0.065\left(\frac{D_{eq}Pe}{L_t}\right)}{1 + 0.04\left(\frac{D_{eq}Pe}{L_t}\right)^{2/3}} \tag{13}$$

where $Pe = Re.\ Pr$

D_{eq} is the equivalent diameter, and L_t is the tube length.

For a coiled heating wire of actual length (l), and coiled length (L_C), the equivalent diameter ($D_{eq} = D_t - d_{eff}$) was found by writing the actual wire volume in terms of the effective diameter d_{eff}

$$\frac{\Pi}{4} d^2 l = \frac{\Pi}{4} d_{deff}^2 \ .\ L_C \tag{14}$$

(d is the actual wire diameter)

i.e., $d_{eff} = \mathrm{d}\sqrt{\frac{l}{L_C}}$ to give

$$D_{eq} = D_t - \mathrm{d}\sqrt{\frac{l}{L_C}}$$

The dependence of the conductive heat loss on the fluid heat capacity Cp, and on the fluid flow rate is shown in Figures 3 and 4.

At low flow rates (particularly), and for fluids of low-heat capacity (e.g., Cp = 1,000 J/kgK,), the heat losses are considerable, and it is evident that *calibration of a flow calorimeter with one fluid of known properties will not apply for another fluid with different properties.*

Equipment and Experimental Procedure

A glass and Teflon calorimeter was designed to be similar to that of the theoretical model shown in Figure 1. The design is shown in Figure 5. The principal element is a coiled nichrome wire heating element suspended in a ±15 cm glass tube of 4.0 mm internal diameter. The nichrome and copper lead-in wires had an identical diameter of 0.40 mm. A vacuum jacket surrounds the tube. The jacketed tube is fitted into Teflon end pieces of the same external diameter as the vacuum tube. The Teflon end pieces contain terminals for the copper wire, as shown. Connection of the inner tube to the two Teflon end pieces is made via sets of two viton o-rings. These produce leak-tight joints, but also good thermal insulation of the flow tube. For the exit section another glass tube of the same diameter, also vacuum insulated, is fitted with a similar set of o-rings into the second Teflon end piece. Miniature Pt-100 temperature sensors are installed as

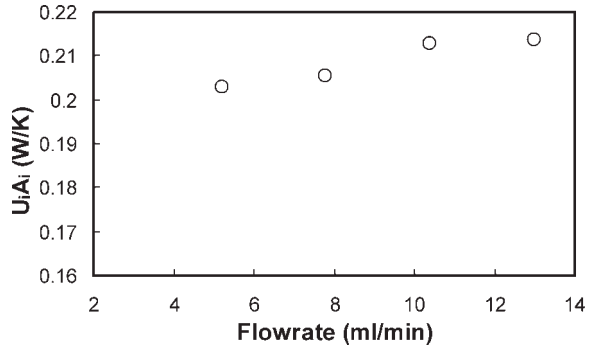

Figure 8. Measured overall heat-transfer coefficient, U_iA_i as a function of flow rate for n-heptane.

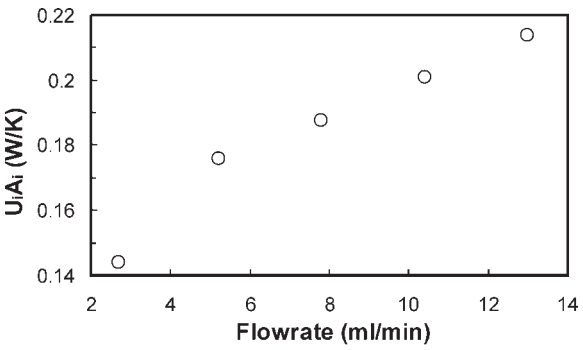

Figure 10. Measured overall heat-transfer coefficient, U_iA_i as a function of flow rate for n-butanol.

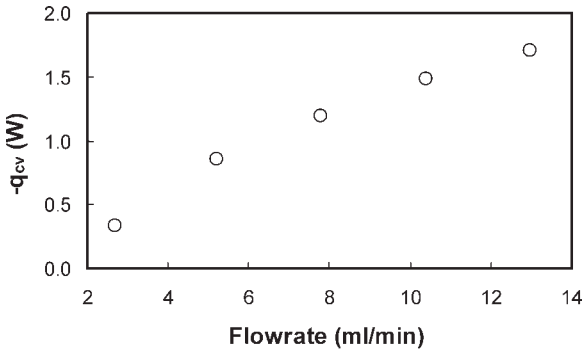

Figure 11. Measured convection heat loss ($q_{cv} = U_iA_i(\Delta T)_{lm}$) as a function of flow-rate for n-butanol.

shown, with care taken to have metal fittings of small thermal capacity for rapid response. To prevent any bath fluid contact with the inner flow tube a few layers of transparent tape (not shown) were wound around the three junctions.

The Pt - 100 sensor installed at the fluid entrance did not, however, reflect the true fluid temperature and temperature readings were found to have some flow rate dependence (probably again due to conductive heat loss from the sensor wires). This was rectified by the modification shown in Figure 6.

The entire assembly, which is quite compact, (see photograph in Figure 7) is suspended in a constant temperature water bath with temperature control to $\pm 0,\ 05^{\circ}C$. Liquid flow was produced with two Beckman model 110A microflow pumps connected in parallel to produce flow rates up to 19 ml/min. Twin pulse-dampeners of our own design, in series, preceded the calorimeter. Experiments were conducted using glass tubes of either 3 mm or 4 mm ID in the calorimeter. Flow rates at a given pump setting were reproducible to ± 0.002g/s.

Instrumentation

The resistance of the temperature sensing elements was measured on a 5 digit Fluke model 8840A multimeter with internal selection and using 4-wire leads. DC power to the heater element was supplied from a programmable Amret model PPS2322 power supply regulated to 0.03% of reading. Measured bath temperatures were accurate to $\pm 0.1^{\circ}C$.

Voltage and current readings, to determine power input were measured on separate Fluke model 8840A digital multimeters. Two series of experiments were performed over a variety of flow rates ranging from 3 to 19 ml/min for five liquids, viz, n-hexane, n-heptane, n-propanol, n-butanol and distilled water. In the first series, power inputs to the heater

Table 1. Overall Heat-Transfer Coefficient U_iA_i for Different Fluids

	U_iA_i (W/K)				
$\dot{V}$ (*ml*/min)	n-Butanol	n-Propanol	n-Hexane	n-Heptane	Water
9	0.19	0.16	0.26	0.20	0.16
15	0.21	0.16	0.34	0.21	0.25

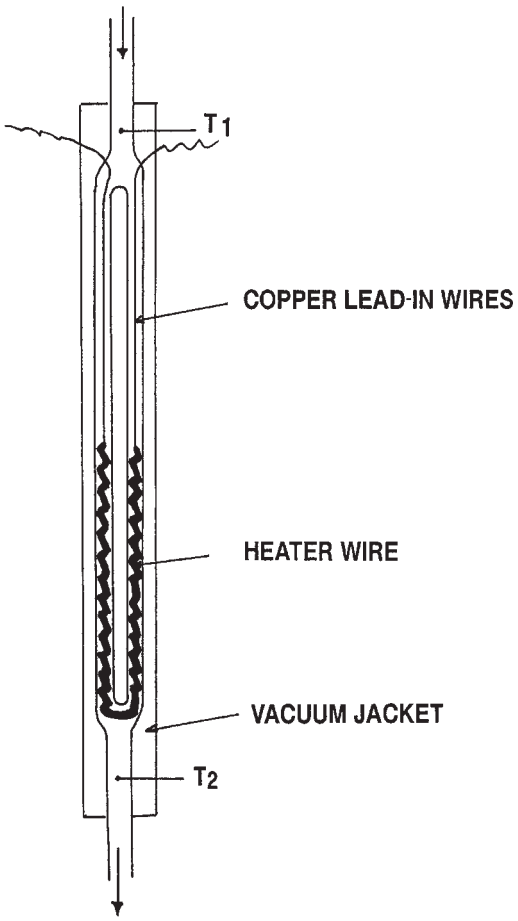

Figure 12. Schematic diagram of a flow calorimeter, which could considerably reduce heat losses through the heater lead-in wires.

elements ranged from about 0.4W to 1.5 W. The second series of experiments was devised to determine overall heat loss from the exterior of the calorimeter assembly to the environment, that is, the water bath in which the assembly was immersed, and to find fluid friction losses (lw_f). In these experiments the experimental fluid was brought to a temperature a few degrees above or below that of the water bath by passage through a coiled tube immersed in another bath. The coiled tube was of sufficient length, as calculated by

Table 2. Conductive Heat Losses q_{HL}: Experimental and Predicted, using n-Propanol Data to Evaluate C'_8, C'_9 and $\overline{x_4}$ in Eq. 12

	Fluid Flow-rate $\dot{V}$ (ml/min) ($q_{HL}/\dot{q}$)%			
	Nominal	$Cp(J/kgK)$*	Experimental	Predicted
n-Heptane	14	2251	13.17	13.68
	16	2251	11.78	12.84
n-Hexane	16	2275	11.78	12.32
	17	2275	10.14	12.32
n-Butanol	12	2406	19.64	16.77
	18	2406	16.13	12.83

*Literature data at 299.7K

Table 3. Conductive Heat Loss (q_{HL}) as a Function of Power Input, $\dot{q}$

	$(q_{HL}/\dot{q})$ %	
$\dot{q}$ (W)	Experimental	Theory
	n-Butanol, $\dot{V}$=18 ml/min	
1.554	16.12	12.80
1.337	16.11	12.82
1.139	16.15	12.83
0.957	16.12	12.85
Average	16.13	12.83
	n-Hexane, $\dot{V}$ = 16 ml/min	
1.152	11.98	12.32
0.969	11.78	12.32
0.802	12.00	12.32
0.648	11.26	12.32
Average:	11.76	12.32

Raal and Webly[7] to ensure a very close approach of the fluid temperature to the bath temperature at all flow rates studied. No electrical energy was supplied to the heater elements.

Estimation of Convective Heat Losses and Fluid Friction

For steady flow of an incompressible fluid and neglecting kinetic and potential energy changes, the macroscopic energy balance, applied across the calorimeter gives for ($\dot{q} = o$)

$$\Delta H = Cp\Delta T + \Delta P/\rho = \frac{U_i A_i (\Delta T)_{lm}}{\dot{m}} \tag{15}$$

For nearly isothermal operation the physical properties Cp and ρ are effectively constant at their average values, and the pressure drop term reflects the frictional energy loss lw_f. For runs at two different but constant temperatures, the friction term, which can be written as

$$\dot{m}\, lw_f = 128L\mu\left(\dot{V}\right)^2/\pi D^4 = K\mu\left(\dot{V}\right)^2,$$

can be eliminated by subtraction using Eq. 15

$$U_i A_i (\Delta T)_{lm(\mathrm{I})} = \dot{m} C_p (\Delta T)_{(\mathrm{I})} - K\mu\left(\dot{V}\right)^2 \tag{15a}$$

$$U_i A_i (\Delta T)_{lm(\mathrm{II})} = \dot{m} C_p (\Delta T)_{(\mathrm{II})} - K\mu\left(\dot{V}\right)^2 \tag{15b}$$

The Roman numerals denote measurements at the two temperatures, but at the same flow rate $\dot{m}$. Thus, a good estimate of the convection loss can be obtained from

$$U_i A_i = \frac{\dot{V}\{\rho_{\mathrm{I}} C_{P\mathrm{I}} \Delta T - \rho_{\mathrm{II}} C_{P\mathrm{II}} \Delta T\}}{(\Delta T)_{lm(\mathrm{I})} - (\Delta T)_{lm(\mathrm{II})}} \tag{16}$$

ΔT in the numerator is the temperature change of the fluid in flowing through the calorimeter tube. Once $U_i A_i$ is known, the friction loss $\dot{m} l w_f$ is found from Eq. 15. (If the two temperatures 1 and 2 are sufficiently different to affect the viscosity adjustments could be made to the flow rate $\dot{V}$ to keep the product $(\dot{V}^2\mu)$ constant.) This elaboration was considered unnecessary for the fluids studied, but may be useful for viscous liquids. Once the convection heat loss $q_{cv} = U_i A_i (\Delta T)_{lm}$, and the frictional energy loss (if not negligible) have been found the conductive heat loss q_{HL}, can be determined from Eq. 17, and compared with predictions obtained from the principal correlating equation, Eq. 12

$$\dot{q} - q_{HL} - q_{cv} = \dot{m} C_p \Delta T + \dot{m}\Delta p/\rho \tag{17}$$

Results and Discussion

Convection heat loss q_{cv} and fluid friction (mlw_f)

Although care was taken in the design of the calorimeter to eliminate convective heat-transfer losses from the calorimeter exterior to its environment, the heat losses were $U_i A_i (\Delta T)_{lm} (= q_{cv})$ not negligible, and were flow rate and fluid property dependent.

Examples of $(U_i A_i)$ as a function of volumetric flow rate are shown in Figures 8 and 10 and q_{cv} Figures 9 and 11.

The values of $U_i A_i$ found for different fluids at two flow rates are compared in Table 1. Although we have measured $U_i A_i$ at several flow rates for all five liquids studied, an average value of 0.23 W/K at 15 mL/min would probably suffice for determining liquid heat capacity unless the highest accuracy is desired. Once q_{cv} is known (at a selected flow rate), the frictional loss can be determined for the fluids measured using known values for the heat capacity Cp, from Eq. 15. Fluid friction was found to be sufficiently small (about 0.02W to 0.12W) to neglect this term in determining conductive heat losses and liquid heat capacities. Convective heat losses were generally much larger, as shown in Figures 9 and 11 for n-butanol and n-heptane, both measured with the 4 mm tube.

Conductive Heat Losses (q_{HL})

To test the theoretical model, as exemplified by the conductive heat loss correlating equation (Eq. 12) q_{HL} was

Table 4. Measured Conductive and Convective Heat Losses, q_{HL} and q_{cv} for Varying Power Inputs, $\dot{q}$: n-butanol

Flow-rate $\dot{V}$- ml/min	Power Input $\dot{q}$ (W)	$T_{out} - T_{in}$ (= $\Delta T/K$)	$U_i A_i$ W/K	q_{cv} (W)	q_{HL} (W)	$\frac{q_{HL}}{\dot{q}}$ %
12.0	1.123	2.441	0.201	0.089	0.228	20.33
12.0	0.943	2.047	0.201	0.077	0.190	20.17
12.0	0.776	1.684	0.201	0.066	0.154	19.89
12.0	0.626	1.361	0.201	0.056	0.122	19.42
18.0	1.554	2.430	0.226	0.100	0.251	16.12
18.0	1.337	2.088	0.226	0.088	0.215	16.11
18.0	1.139	1.773	0.226	0.077	0.184	16.15
18.0	0.957	1.487	0.226	0.067	0.154	16.12

Table 5. Measured Conductive and Convective Heat Losses, $q_{HL}/\dot{q}$ for Varying Power Inputs, $\dot{q}$: water

Flow-rate $\dot{V}$ ml/min	Power Input $\dot{q}$ (w)	$T_{out} - T_{in}$ (= $\Delta T/K$)	U_iA_i W/K	q_{cv} (W)	q_{HL} (W)	$\frac{q_{HL}}{\dot{q}}$ %
7.00	1.549	2.576	0.179	0.083	0.381	24.59
7.00	1.337	2.218	0.179	0.073	0.329	24.62
7.00	1.138	1.896	0.179	0.065	0.275	24.15
7.00	0.954	1.594	0.179	0.056	0.227	23.78
19.00	1.549	1.167	0.281	0.069	0.147	9.46
19.00	1.337	1.011	0.281	0.061	0.120	9.00
19.00	1.137	0.865	0.281	0.054	0.094	8.28
19.00	0.955	0.729	0.281	0.048	0.074	7.73

measured in several series of experiments at a few flow rates, and for electrical energy inputs ranging from about 0.5 to 1.5W. With $\dot{q}$ and q_{cv} known (the latter from the experiments described earlier) q_{HL} was computed from

Eq. 17a for known values of Cp

$$q_{HL} = \dot{q} - q_{cv} - \dot{m}Cp\Delta T \tag{17a}$$

Results are shown in Tables 2 to 4, and are in agreement with the predictions shown in Figures 3 and 4. i.e., fractional heat losses decrease with increasing flow rates, and also decrease with increasing heat capacity Cp (Table 2). Other fluid properties, however, contained in Eq. 12 through the heat-transfer coefficient h, and the density ρ will also influence the conductive heat loss. The conductive heat losses were only mildly sensitive to the energy input levels, and are quite large as also suggested by the predictions in Figures 3 and 4. For distilled water (Table 5) measured conductive heat losses also follow the trends shown in Figures 3 and 4, i.e., q_{HL} decreases with flow rate increase and with heat capacity increase. Predicted values from Eq. 12, however, did not match the measured values for unknown reasons. Possibly the much higher thermal conductivity for water is not adequately accounted for in the convective heat-transfer correlation (Eq. 13).

Comparison of Measured and Predicted Heat Losses

Conductive heat losses were *predicted* using Eq. 12. The three constants C'_8, C'_9, and $\overline{x_4}$ were evaluated from the heat loss measurements for n-propanol over a range of flow rates and energy inputs, with $X = 3.5$, determined from the calorimeter physical properties. These values were then used in Eq. 12 to predict conductive heat losses for the other fluids at several energy inputs and for a few flow rates. Despite the disconcertingly large values for C'_8, and C'_9 ($>10^8$ with $\overline{x_4} = 0.2547$) very good predictions for q_{HL} were obtained for other liquids, as shown in Tables 2 and 3. Since Eq. 12 contains the heat capacity, a trial and error procedure is required in general in which Eqs. 12 and 17a are used alternatively until convergence is obtained for Cp. Measurements from the 3 mm and 4 mm ID tubes revealed no substantial differences in conductive heat losses or Cp values.

Heat Capacity Measurements

With values for X, C'_8, C'_9 and $\overline{x_4}$ fixed heat capacities were measured for n-heptane, n-hexane and n-butanol, using Eqs. 12 and 17a alternatively in the trial-and error procedure until converged values were obtained for q_{HL} and Cp. The measured values were then compared with literature data as shown in Table 6. Agreement is very good with errors ranging from 0.58% to 6.5% (depending on which literature data are assumed to be correct).

Conclusion

For a five-zone model flow calorimeter, realistic and novel longitudinal temperature distributions in the flowing fluid and in the heater element were obtained from solutions of the governing third-order differential equation in the fluid temperature T.

Table 6. Measured Fluid Heat Capacities, Using Eq. 12 for Conductive Heat Losses and Calibration with n-propanol

Nominal Flow Rate (ml/min)	Starting Value of Cp (J/kgK)	Convergent Value of Cp (J/kgK)	Literature Value of Cp (Messerly et al.[18])	% Error	Literature Value of Cp (Reklaitis[19])	% Error
		Experimental fluid: n-heptane Tube ID: 4 mm (all fluids)				
14.0	1000	2286.17	2250.51	1.58	2253.70	1.44
16.0	1000	2266.79	2250.45	0.72	2253.62	0.58
		Experimental fluid: n-hexane				
16.0	1000	2250	2275	1.06	2276	1.11
17.0	1000	2246	2275	2.26	2276	2.31
		Experimental fluid: n-butyl alcohol				
12.0	1000	2509	2357	6.44	2406	4.29
18.0	1000	2478	2357	5.13	2406	3.00

All C_p values at 299.7K and atmospheric pressure.

Decomposition of the large matrix of algebraic equations, obtained from application of realistic boundary conditions, permitted evaluation of the 13 integration constants for chosen calorimeters characteristics, fluid flow rate and physical properties.

Conductive heat losses (q_{HL}) were large, principally at the calorimeter exit and flow rate and fluid property dependent. They increased rapidly with decrease in fluid flow rate and heat capacity, giving useful guidance in the selection of fluid flow rate. The explicit dependence of q_{HL} on calorimeter characteristics and on fluid flow rate and properties, and their convenient separation was achieved with the correlating equation (Eq.12). Predicted conductive heat losses for several organic liquids were in satisfactory agreement with measured ones for varying flow rates, and their use in Eq. 17a produced *Cp* measurements ranging from good to excellent in comparison with literature values.

Calibration of a flow calorimeter with one fluid of known Cp cannot satisfactorily be used for another with different properties

For distilled water conductive heat losses followed the same dependence on flow rate and heat capacity as those for organic liquids but predicted values q_{HL} did not match the measured ones. This was possibly due to the much larger thermal conductivity of water, not adequately reflected in the heat-transfer correlation (Eq. 13). In Figure 12 is shown a diagram of a flow calorimeter which could considerably reduce conductive heat losses through the heater lead-in wires.

Finally, the dimensionless groups in Eq. 1, Appendix 1 could be used for empirical correlations of q_{HL} in a less structured alternative approach. These groups are

$$\left[\frac{hPf(\Delta x)_3}{C_H}\right],\ \left[\frac{hPf^2(\Delta x_3)^2}{ka}\right] \text{ and } \left[\frac{(\Delta x_3)^3 \dot{q} h P^2 f^3}{\dot{m} C p k a T}\right]$$

($\dot{q}$ in the last group is the heat generated per unit area of the heater surfaces W/m^2).

Acknowledgments

The authors are indebted to Bavanethan Pillay for his formulation and solution of the equation matrix for an earlier 5-zone calorimeter model.

Literature Cited

1. Raal JD, Gadodia V, Ramjugernath D, Jalari R. New developments in differential ebulliometry: experimental and theoretical. *J Mol Liq*. 2006;125:45–57
2. Zabranski M, Ruzicka V, Majei V, Domalski E S. Heat capacities of liquids vol. I and II, critical review and recommended values. *J Phys Chem Ref. Data monograph* 6;1996.
3. Domalski ES, Hearing ED. Heat capacities and entropies of organic compounds in the condensed phase. *J Phys Chem Ref Data*. 1996;25:1–5.
4. Poling BE, Prausnitz JM, O' Connell JP. *The properties of gases and liquids*. 5th ed. Boston: Mcgraw-Hill; 2001.
5. Diedrichs A, Gmehling J. Prediction of liquid heat capacities by the group contribution equation of state. *Fluid Phase Equilib*. 2006; 248:56–59
6. Diedrichs A, Gmehling J. Measurement of heat capacities of ionic liquids by differential scanning calorimetery. *Fluid Phase Equilib*. 2006;244:68–77
7. Raal, JD, Webley PA. Microflow calorimeter design for heats of mixing. *AIChE J*. 1987;33:604–618
8. Raal JD. Separation of fluid frictional energy and heats - of - mixing in a flow calorimeter *AIChE J*. 1993;39:715–719.
9. Picker P, Leduc P-A, Philip PR, Desnoyers JE. Heat capacity measurement by flow calorimetry. *J Chem Thermodyn*. 1971;3:631–642.
10. Picker P. New concepts in design and applications of flow microcalorimetry. *Can Res Dev*. 1974;7(1):11–16.
11. Smith-Magowan D, Wood RH. Heat capacity of aqueous sodium chloride from 320 to 600 K measured with a new flow calorimeter. *J Chem Thermodyn*. 1981;13:1047–1073.
12. Rogers PSZ, Pitzer KS. High-temperature thermodynamic properties of aqueous sodium sulfate solutions. *J Phys Chem*. 1981;85:2886–2895.
13. Rogers PSZ, Duffy CJ. Comparison of calibration methods for flow heat-capacity calorimeters and heat capacities of concentrated NaC1 (aq) to 598 K. *J Solution Chem*. 1989;21:595–614.
14. Saitoh A, Nakagawa S, Sato H, Watanabe K. J. Isobaric heat capacity data for liquid HFC-134a. *Chem Eng Data*. 1990;35:107–110.
15. Nakagawa S, Holi T, Saito H, Watanabe K. Isobaric heat capacity for liquid 1-chloro 1, 1 difluoroethane and 1, 1 difluoroethane. *J Chem Eng Data*. 1993;38:70–74.
16. Brouckaert CJ. School of Chemical Engineering, University of K-Z-Natal. Personal communication; 2005.
17. Mills F. *Heat transfer*. Boston: Irwin; 1992
18. Messerly JF, Guthrie GB, Todd SS, Finke HL. Low temperature thermal data for n-pentane n-heptadecane and n-octadecane. *J Chem Eng Data*. 1967;12:336–346.
19. Reklaitis GV. *Introduction to Material and Energy Balances*. New York: John Wiley & Sons; 1983.
20. Yaws CL, Miller JW. Heat capacities of liquids. *Chem Eng*. 1976;83:129–13
21. Raznjevic K. Handbook of thermodynamic tables and charts. Washington DC: Hemisphere; 1976.

Appendix 1: Solution of Equations

In terms of dimensionless variables in Eqs. 4 to 6, Eq. 3 becomes

$$\frac{d^3\overline{T}}{d\overline{x}^3} + \left(\frac{hPf + U\pi D}{C_H}\right)\Delta x_3\left(\frac{d^2\overline{T}}{d\overline{x}^2}\right) - \left(\frac{hPf^2(\Delta x_3)^2}{ka}\right)\left(\frac{d\overline{T}}{d\overline{x}}\right) - \frac{UhPf^2(\Delta x_3)^3}{kaC_H}(\pi D)\overline{T} + \frac{(\Delta x_3)^3}{T_{ref}}\left(\frac{\dot{q}h\dot{P}^2f^3}{kaC_H}\right) = 0$$

$$\left[T_{ref} = (T - T_c)_{ideal} = \frac{\dot{q}}{\dot{m}\dot{C}_P}\right] \quad \text{(A1)}$$

Nondimensional Boundary Conditions

Boundary conditions in dimensionless form, requiring that there be no discontinuities in temperature or heat flux in the bimetal wire or fluid in passing from one zone to another, are as follows

$$(1)\ \overline{x} = 0 \qquad : \overline{T} = 0, \bar{t} = 0, \quad \text{(A2a)}$$

$$(2)\ \overline{x} = \frac{x_1}{\Delta x_3} \quad : \overline{T}_{\mathrm{I}} = \overline{T}_{\mathrm{II}}, \bar{t}_{\mathrm{I}} = \bar{t}_{\mathrm{II}}, \left(\frac{d\bar{t}}{d\overline{x}}\right)_{\mathrm{I}} = \left(\frac{d\bar{t}}{d\overline{x}}\right)_{\mathrm{II}} \quad \text{at } \overline{x} = \overline{x}_1 \quad \text{(A2b)}$$

$$(3)\ \overline{x} = \frac{x_2}{\Delta x_3} \quad : \overline{T}_{\mathrm{II}} = \overline{T}_{\mathrm{III}}, \bar{t}_{\mathrm{II}} = \bar{t}_{\mathrm{III}}, k_1\left(\frac{d\bar{t}}{d\overline{x}}\right)_{\mathrm{II}} = k_2\left(\frac{d\bar{t}}{d\overline{x}}\right)_{\mathrm{III}} \quad \text{at } \overline{x} = \overline{x}_2 \quad \text{(A2c)}$$

$$(4)\ \bar{x} = \frac{x_3}{\Delta x_3} \quad : \overline{T}_{\mathrm{III}} = \overline{T}_{IV}, \bar{t}_{\mathrm{III}} = \bar{t}_{IV}, k_2\left(\frac{d\bar{t}}{d\bar{x}}\right)_{\mathrm{III}} = k_1\left(\frac{d\bar{t}}{d\bar{x}}\right)_{IV} \quad \text{at } \bar{x} = \bar{x}_3 \quad \text{(A2d)}$$

$$(5)\ \bar{x} = \frac{x_4}{\Delta x_3} \quad : \overline{T}_{IV} = \overline{T}_{V}, \bar{t}_{IV} = \bar{t}_{V}, \left(\frac{d\bar{t}}{d\bar{x}}\right)_{IV} = \left(\frac{d\bar{t}}{d\bar{x}}\right)_{V} \quad \text{at } \bar{x} = \bar{x}_4 \quad \text{(A2e)}$$

$$(6)\ \bar{x} = \frac{x_5}{\Delta x_3} \quad : \bar{t} = 0, \qquad \text{at } \bar{x} = \bar{x}_5 \quad \text{(A2f)}$$

Here k_1 and k_2 are the thermal conductivities of copper and nichrome, respectively, assumed constant over the small temperature ranges normally involved.

Solutions of Eq. 1

For the case of $U = 0$, Eq. A1 can be reduced to a second-order ordinary differential equation with constant coefficients, since it does not contain the dependent variable $\overline{T}$ explicitly. Thus, letting

$$\begin{aligned} &\mathrm{Z} = \frac{d\overline{T}}{d\bar{x}} \text{ Gives :} \\ &\frac{d^2\mathrm{Z}}{d\bar{x}^2} + B\frac{d\mathrm{Z}}{d\bar{x}} - m^2\mathrm{Z} + E = 0 \end{aligned} \quad \text{(A3)}$$

where

$$B = \frac{hPf\Delta x_3}{C_H} \quad \text{(A3a)}$$

$$m_2^2 = \frac{hPf^2(\Delta x_3)^2}{k_2 a} \quad \text{(A3b)}$$

$$E = (\Delta x_3)^3 \frac{\dot{q}\, hP^2 f^3}{k_2 a C_H} \quad \text{(A3c)}$$

The solution of Eq. A3 is straightforward.

For zone 3 $q \neq o$, $h \neq o$, and we obtain

$$Z = \frac{d\overline{T}}{d\bar{x}} = C_4' e^{-q'\bar{x}} + C_5' e^{q_2'\bar{x}} + \frac{\dot{q}(\Delta x_3)\mathrm{P}f}{C_H \overline{T}_{ref}} \quad \text{(A4)}$$

and, hence, the dimensionless fluid temperature distribution

$$\overline{T} = C_4 \frac{e^{-q_1'\bar{x}}}{-q_1'} + C_5 \frac{e^{q_2'\bar{x}}}{q_2'} + \dot{q}\frac{\Delta x_3 Pf}{C_H T_{ref}}\bar{x} + C_6 \quad \text{(A5)}$$

$\dot{q}_1$ and $\dot{q}_2$ are functions only of the dimensionless groups B and m_2. For zones other than 3, $\dot{q} = o = E$, and the thermal conductivity of the lead-in wires k_1 replaces k_2. q_1' and q_2' are given by

$$q_1' = \frac{1}{2}\left\{B + \sqrt{B^2 + 4m_2^2}\right\}$$
$$q' = \frac{1}{2}\left\{-B + \sqrt{B^2 + 4m_2^2}\right\}$$

Since both B and m_2^2 are >0, the aforementioned are real and positive roots.

Similar but simpler solutions are obtained for zones 1, 2, 4 and 5, and involve several additional constants. The application of the boundary conditions, thus, produces a large system of linear equations containing 13 integration constants C_1 to C_{13}. The matrix of equations is shown in Appendix 2. The quantities appearing in the matrix have the following definitions

$$B = \left(\frac{hPf\Delta x_3}{C_H}\right)$$

$$m_1^2 = \left(\frac{hPf^2(\Delta x_3)^2}{k_1 a}\right) \qquad [k_1\text{: } copper]$$

$$m_2^2 = \left(\frac{hPf^2(\Delta x_3)^2}{k_2 a}\right) \qquad [k_2\text{: } nichrome]$$

$$q_1 = \frac{1}{2}\left(B + \sqrt{B^2 + 4m_1^2}\right)$$

$$q_2 = \frac{1}{2}\left(-B + \sqrt{B^2 + 4m_1^2}\right)$$

$$q_1' = \frac{1}{2}\left(B + \sqrt{B^2 + 4m_2^2}\right)$$

$$q_2' = \frac{1}{2}\left(-B + \sqrt{B^2 + 4m_2^2}\right)$$

$$C_H = \dot{m}\, C_P$$

$$T_{ref} = (T - T_C)_{ideal} = \frac{\dot{q}}{\dot{m}\, C_p}$$

Appendix 2: The Coefficient Matrix

c_1	c_2	c_3	c_4	c_5	c_6	c_7	c_8	c_9	c_{10}	c_{11}	c_{12}	c_{13}	Constant term
0	$\frac{e^{-q_1\bar{x}_1}}{-q_1}$	$\frac{e^{q_2\bar{x}_1}}{q_2}$	1	0	0	0	0	0	0	0	0	0	0
$-\bar{x}_1$	$\frac{e^{-q_1\bar{x}_1}}{-q_1} + \frac{C_H e^{-q_1\bar{x}_1}}{hPf(\Delta x_3)}$	$\frac{e^{q_2\bar{x}_1}}{q_2} + \frac{C_H e^{q_2\bar{x}_1}}{hPf(\Delta x_3)}$	1	0	0	0	0	0	0	0	0	0	0
-1	$e^{-q_1\bar{x}_1} - \frac{C_H q_1 e^{-q_1\bar{x}_1}}{hPf(\Delta x_3)}$	$e^{q_2\bar{x}_1} + \frac{C_H q_2 e^{q_2\bar{x}_1}}{hPf(\Delta x_3)}$	0	0	0	0	0	0	0	0	0	0	0
0	$\frac{e^{-q_1\bar{x}_2}}{-q_1}$	$\frac{e^{q_2\bar{x}_2}}{q_2}$	1	$\frac{e^{-q_1'\bar{x}_2}}{q_1'}$	$\frac{e^{q_2'\bar{x}_2}}{-q_2'}$	-1	0	0	0	0	0	0	$\dot{q}\frac{(\Delta x_3)Pf}{C_H T_{ref}}\bar{x}_2$
0	$e^{-q_1\bar{x}_2}$	$e^{q_2\bar{x}_2}$	0	$-e^{-q_1'\bar{x}_2}$	$-e^{q_2'\bar{x}_2}$	0	0	0	0	0	0	0	$\dot{q}\frac{(\Delta x_3)Pf}{C_H T_{ref}}$
0	$k_1 e^{-q_1 x_2} - \frac{k_1 C_H q_1 e^{-q_1\bar{x}_2}}{hPf(\Delta x_3)}$	$k_1 e^{q_2\bar{x}_2} + \frac{k_1 C_H q_2 e^{q_2\bar{x}_2}}{hPf(\Delta x_3)}$	0	$-k_2 e^{-q_1'\bar{x}_2} + \frac{k_2 C_H q_1' e^{-q_1'\bar{x}_2}}{hPf(\Delta x_3)}$	$-k_2 e^{q_2'\bar{x}_2} - \frac{k_2 C_H q_2' e^{q_2'\bar{x}_2}}{hPf(\Delta x_3)}$	0	0	0	0	0	0	0	$k_2\,\dot{q}\frac{(\Delta x_3)Pf}{C_H T_{ref}}$
0	0	0	0	$\frac{e^{-q_1'\bar{x}_3}}{q_1'}$	$\frac{e^{q_2'\bar{x}_3}}{-q_2'}$	-1	$\frac{e^{-q_1\bar{x}_3}}{-q_1}$	$\frac{e^{q_2\bar{x}_3}}{q_2}$	1	0	0	0	$\dot{q}\frac{(\Delta x_3)Pf}{C_H T_{ref}}\bar{x}_3$
0	0	0	0	$-e^{-q_1'\bar{x}_3}$	$-e^{q_2'\bar{x}_3}$	0	$e^{-q_1\bar{x}_3}$	$e^{q_2\bar{x}_3}$	0	0	0	0	$\dot{q}\frac{(\Delta x_3)Pf}{C_H T_{ref}}$
0	0	0	0	$-k_2 e^{-q_1'\bar{x}_3} + \frac{k_2 C_H q_1' e^{-q_1'\bar{x}_3}}{hPf(\Delta x_3)}$	$-k_2 e^{q_2'\bar{x}_3} - \frac{k_2 C_H q_2' e^{q_2'\bar{x}_3}}{hPf(\Delta x_3)}$	0	$k_1 e^{-q_1\bar{x}_3} - \frac{k_1 C_H q_1 e^{-q_1\bar{x}_3}}{hPf(\Delta x_3)}$	$k_1 e^{q_2\bar{x}_3} + \frac{k_1 C_H q_2 e^{q_2\bar{x}_3}}{hPf(\Delta x_3)}$	0	0	0	0	$k_2\,\dot{q}\frac{(\Delta x_3)Pf}{C_H T_{ref}}$
0	0	0	0	0	0	0	$\frac{e^{-q_1\bar{x}_4}}{-q_1}$	$\frac{e^{q_2\bar{x}_4}}{q_2}$	1	0	0	-1	0
0	0	0	0	0	0	0	$\frac{e^{-q_1\bar{x}_4}}{-q_1} + \frac{C_H e^{-q_1\bar{x}_4}}{hPf(\Delta x_3)}$	$\frac{e^{q_2\bar{x}_4}}{q_2} + \frac{C_H e^{q_2\bar{x}_4}}{hPf(\Delta x_3)}$	1	$-\bar{x}_4$	-1	0	0
0	0	0	0	0	0	0	$e^{-q_1\bar{x}_4} - \frac{C_H q_1 e^{-q_1\bar{x}_4}}{hPf(\Delta x_3)}$	$e^{q_2\bar{x}_4} + \frac{C_H q_2 e^{q_2\bar{x}_4}}{hPf(\Delta x_3)}$	0	-1	0	0	0
0	0	0	0	0	0	0	0	0	0	$\bar{x}_5$	1	0	0

Manuscript received Mar. 26, 2008, revision received July 14, 2008, and final revision received Sept. 10, 2008.